ADVANCED ENERGY MATERIALS
www.advenergymat.de



# Mixed Phase Solid-State Plastic Crystal Electrolytes Based on a Phosphonium Cation for Sodium Devices

*Faezeh Makhlooghiazad, Daniel Gunzelmann, Matthias Hilder, Douglas R. MacFarlane, Michel Armand, Patrick C. Howlett, and Maria Forsyth**

**Na batteries are seen as a feasible alternative technology to lithium ion batteries due to the greater abundance of sodium and potentially similar electrochemical behavior. In this work, mixed phase electrolyte materials based on solid-state compositions of a *tri*methylisobutylphosphonium ($P_{111i4}$) bis(*tri*fluromethanesulphonyl)amide ($NTf_2$) organic ionic plastic crystal (OIPC) and high concentration of $NaNTf_2$ that support safe, sodium metal electrochemistry are demonstrated. A Na symmetric cell can be cycled efficiently, even in the solid state (at 50 °C and 60 °C), for a 25 mol% ($P_{111i4}NTf_2$)–75 mol% $NaNTf_2$ composition at 0.1 mA cm$^{-2}$ for 100 cycles. Thus, these mixed phase materials can be potentially used in Na-based devices under moderate temperature conditions. It is also investigated that the phase behavior, conductivity, and electrochemical properties of mixtures of $NaNTf_2$ with this OIPC. It is observed that these mixtures have complex phase behavior. For high compositions of the Na salt, the materials are solid at room temperature and retain a soft solid consistency even at 50 °C with remarkably high conductivity, approaching that of the pure ionic liquid at 50 °C, i.e., $10^{-3}$–$10^{-2}$ S cm$^{-1}$.**

## 1. Introduction

Organic ionic plastic crystals (OIPCs) are a class of materials that have recently been shown to be good candidates as solid-state electrolytes for electrochemical devices including lithium batteries,[1–9] solar cells,[10–12] and fuel cells.[13–15] The term 'plastic' reflects the high degree of mobility, and thus deformability under low applied stress, that is observed in these materials in one or more of the sub-melting phases. Typically, plastic crystals have one or more solid–solid phase transitions before the final melt with the final entropy of melting ($\Delta S_f$) being less than 20 kJ mol$^{-1}$ as defined by Timmermans' criterion.[16] The presence of more disorder in the higher temperature OIPC phases, results in the creation of vacancies and extended defects that ultimately lead to the diffusional motions that result in the plasticity. These diffusive motions also lead to significant ionic conductivity which make these materials excellent candidates as safe electrolytes for electrochemical devices. Furthermore, mixing additional salts into the OIPC matrix usually leads to significant enhancement of the conductivity,[2,8,9,17,18] such that these mixtures become useful solid-state electrolyte materials in devices including lithium batteries and dye sensitized solar cells.

The ammonium (including pyrrolidinium and *tetra*alkyl ammonium) based families of OIPCs with different anions, e.g., $NTf_2$, $N(CN)_2$, $BF_4$, and $PF_6$ have been extensively studied both at the fundamental level,[2,5,19–28] and in devices.[7–9,17,29,30] Recently, some phosphonium-based OIPC materials have also been investigated.[9,31,32] Phosphonium cations in ionic liquids have been suggested to produce favorable properties compared to their ammonium analogues, including higher electrochemical stability,[33–36] and the ability to stabilize the superoxide species,[37,38] which is beneficial for reversible metal-air battery applications such as in Li-air or Na-air devices.[39,40]

Sodium salt mixtures with OIPCs have only been reported, by some of us, recently for the case of $C_2$mpyr$NTf_2$[41] and $C_2$mpyrDCA[25] (where $C_2$mpyr is the methyl ethyl pyrrolidinium cation). In both cases, a eutectic transition well above room temperature (63 °C and 88 °C, respectively) exists and thus these mixtures are solid for an extensive temperature range. While the solid-state conductivity for some compositions in this family of materials is significant, it was not yet high enough for their applications in sodium devices. In this paper, we explore the higher $NaNTf_2$ compositions in more detail and show that high conductivities are obtained in these mixtures, even while maintaining a solid state. This allows successful cycling of Na/Na$^+$ from this material, thus paving the way towards solid-state sodium-based energy storage devices. A combination of differential scanning calorimetry

F. Makhlooghiazad, Dr. D. Gunzelmann, Dr. M. Hilder, Prof. M. Armand, Prof. P. C. Howlett, Prof. M. Forsyth
Institute for Frontier Materials
Deakin University
Waurn Ponds Campus
75 Pigdons Road, Geelong, Victoria 3220, Australia
E-mail: Maria.Forsyth@deakin.edu.au
Prof. D. R. MacFarlane
School of Chemistry
Monash University
Victoria 3800, Australia
Prof. M. Armand
CIC Energigune Energy Cooperative Research Centre
C/Albert Einstein 48, CP 01510, Spain

DOI: 10.1002/aenm.201601272

 © 2016 WILEY-VCH Verlag GmbH & Co. KGaA, Weinheim 

(DSC), conductivity, scanning electron microscope (SEM), nuclear magnetic resonance (NMR) spectroscopy, and electrochemical methods are also employed to investigate the phase behavior, transport, and electrochemistry in these new materials.

## 2. Results and Discussion

### 2.1. Phase Behavior as Determined by Thermal Analysis in OIPC/ $NaNTf_2$ Mixtures

DSC heating traces for $(1-x)P_{111i4}NTf_2$ – $(x)NaNTf_2$ for $x = 0$, 25, 80, and 100, are presented in **Figure 1**a. The melting temperatures of pure $P_{111i4}NTf_2$ and $NaNTf_2$ are 40 °C and 257 °C, respectively. Pure $P_{111i4}NTf_2$ shows one solid–solid phase transition at –48 °C before melting at 40 °C with a final entropy of melting of 45 J $mol^{-1}$ $K^{-1}$. Thus, the pure $P_{111i4}NTf_2$ presents as phase I over a wide range of temperatures from –48 °C to 40 °C, however, this relatively high remaining melting entropy for the pure OIPC is higher than the Timmermans' criterion for molecular plastic crystals,[16] Therefore the degree of plasticity and ion dynamics in this system may not be as high as those OIPC materials such as $P_{1444}FSI$,[9] $P_{1224}PF_6$,[32] and $P_{1224}SCN$[36] with final entropy of melting significantly less than 20 J $mol^{-1}$ $K^{-1}$ (the lower final entropy of melting indicating the presence of greater motional degrees of freedom in the solid-state sub-melting). Adding $NaNTf_2$ to the pure OIPC lowers the melting point of the mixed system compared to the pure material (Figure S1, Supporting Information and Figure 1a).

This effect has been also reported previously in the two binary systems containing $NaNTf_2/C_2mpyrNTf_2$[41] and $NaN(CN)_2/C_1mpyrN(CN)_2$.[25] Mixing with the sodium salt also introduces an additional endothermic peak just before the final melting point at 36 ± 0.5 °C. The enthalpy of this peak is maximum for the composition of 5 mol% $NaNTf_2$, and at this composition, this is the only peak observed therefore we suggest this represents a eutectic transition.[42] Thus, at temperatures higher than this eutectic temperature ($T_e$ = 36 °C), the 5 mol% $NaNTf_2$ sample is totally liquid, whereas below $T_e$ it solidifies into two different solid phases. For the 25 mol% composition, there are two sharp transitions at 36 °C and 48 °C which correspond to a solid–solid phase transition and a peritectic transition.[42] A very small final liquidus transition is observed at 75 °C, which is also verified visually as the final melt. Similarly, at higher $NaNTf_2$ compositions, a sharp transition is observed at 48 °C above which the material consists of two phases, one liquid phase and the other an $NaNTf_2$ rich phase whose final melting point approaches pure $NaNTf_2$ ($T_m$ = 257 °C). The DSC thermal traces for a number of additional compositions is presented in Figure S1 in the Supporting Information.

The corresponding phase diagram for the $P_{111i4}NTf_2/NaNTf_2$ binary systems, extracted from careful analyses of DSC data as well as monitoring the visual melting point of some compositions is presented in Figure 1b. The phase diagram for the $P_{111i4}NTf_2/NaNTf_2$ binary systems has three main features; the first being the presence of the eutectic transition at 36 °C with the composition of 5 mol% $NaNTf_2$ which undergoes the $L \rightarrow A + A_4B$ reaction (A is an OIPC rich phase and we denote $A_4B$ as an intermediate compound). This intermediate compound appears to be a mixed salt crystalline phase at 20 mol% $NaNTf_2$ (stoichiometry $4/1(P_{111i4}NTf_2/NaNTf_2)$), $A_4B$, that is evident in the phase diagram. Finally, an incongruous melting of this new crystalline phase at 45 °C, a result of a peritectic reaction ($L + B' \rightarrow A_4B$ where B′ is the sodium salt rich phase) is present. Below the eutectic transition two distinct solid phases form, one of which belongs to the OIPC rich phase and the other one is the intermediate compound. The liquidus behavior beyond $A_4B$ also suggests that additional compounds may exist, e.g., $A_2B$ or AB, but these were not readily detected in the DSC thermograms nor was there clear evidence of these from other characterization methods discussed. Therefore, the phase diagram presented in Figure 1b may not represent the complete behavior for this system, but nonetheless is indicative the complexity of these mixtures.

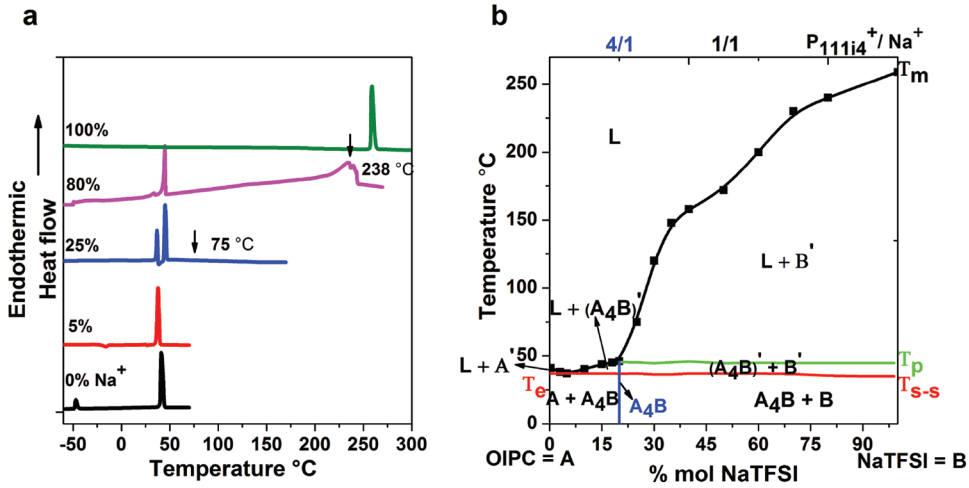


**Figure 1.** a) DSC traces of pure $P_{111i4}NTf_2$ and $NaNTf_2$ and some of their mixtures. b) Measured phase behavior for $P_{111i4}NTf_2$ and $NaNTf_2$ binary systems. The solid–solid transition observed for the $NaNTf_2$ rich side is nearly coincident with the eutectic transition observed for OIPC rich region.


© 2016 WILEY-VCH Verlag GmbH & Co. KGaA, Weinheim

### 2.2. Ionic Conductivity

The temperature-dependent ionic conductivity of the pure $P_{111i4}NTf_2$ and its mixtures with $NaNTf_2$ are presented in **Figure 2** for 0, 5, 20, 25, 50, and 75 mol% $NaNTf_2$ compositions. In the case of the pure sample, the conductivity increases gradually from $10^{-8.5}$ S cm$^{-1}$ at 15 °C to $10^{-4.8}$ S cm$^{-1}$ at 40 °C, and after the melting point at 40 °C increases sharply, reaching $10^{-2.3}$ S cm$^{-1}$. Upon the addition of 5 mol% $NaNTf_2$ to the pure $P_{111i4}NTf_2$ OIPC, the conductivity increases over the entire temperature range, with a sharp rise at 36 °C, most likely due to the eutectic transition which leads to the presence of a liquid phase within the solid matrix. A similar increase in conductivity at the eutectic temperature was reported previously for a Li-doped OIPC.[43] A similar sharp increase in conductivity at 36 °C is also observed for the other compositions (20, 25, and 50 mol%), however, according to the phase diagram these do not undergo a eutectic transition, instead this rise in conductivity follows the solid–solid phase transition which was observed in the DSC traces. Moreover, a two-step increase in conductivity is observed in 20, 25, and 50 mol%; the first conductivity step is attributed to the solid–solid phase transition as we have just discussed and the second (at 45 °C) is related to the peritectic transition. 25 and 50 mol% exhibit a higher ionic conductivity at temperatures lower than 36 °C (below the eutectic and solid–solid phase transition) compared to the other measured compositions (around 3 orders of magnitude higher ionic conductivity is obtained at 30 °C compared to pure OIPC). While both 50 and 25 mol% samples are two-phase materials at all temperatures, the 50 mol% sample shows lower conductivity at temperatures beyond the peritectic point in contrast with 25 mol%. This is because at these temperatures up until the final melting (or liquidus point) for each sample, the 50 mol% sample consists mostly of a solid phase in comparison with the 25 mol% material which would be predominantly liquid phase, in accordance with the phase diagram in Figure 1b. Interestingly, for 75 mol%, a smoother conductivity trend is observed with increasing temperature although the final values above the peritectic transition are somewhat lower than the other compositions, again due to a lesser content of liquid phase (photo in Figure 2) and possible tortuosity for ion diffusion in the material. Indeed, at this composition, at 50 °C, the material presents mostly as a solid waxy substance.

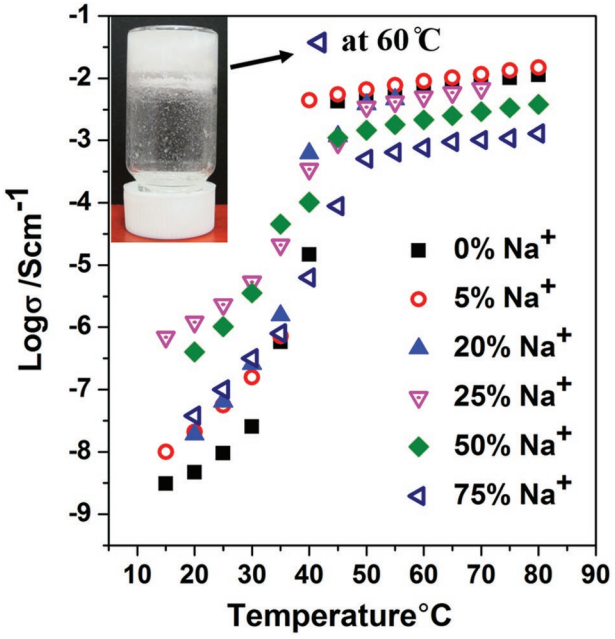


**Figure 2.** Ionic conductivity of $P_{111i4}NTf_2$ electrolytes with different concentrations of $NaNTf_2$.

### 2.3. Na Electrochemistry in the Mixed Phase Electrolytes

#### *2.3.1. Cyclic Voltammetry*

The cyclic voltammogram of 25 mol% $NaNTf_2$ in $P_{111i4}NTf_2$ at 50 °C using a Cu working electrode (which has previously been demonstrated to be a good substrate choice for sodium deposition),[44] is presented in **Figure 3**. This demonstrates the ability of these electrolytes to support reversible reduction and oxidation reactions for the $Na/Na^+$ couple. We examine this electrochemistry further below.

#### *2.3.2. Sodium Transference Number*

The portion of the current carried by Na ions is the Na transference number. The transference number in a symmetric cell was determined using the Bruce–Vincent–Evans method:[45,46]

$$t_{Na}^{+} = \frac{I_s\left(\Delta V - I_0 R_0\right)}{I_0\left(\Delta V - I_s R_s\right)}$$

The response of the Na symmetric cell containing 25 mol% $NaNTf_2$ in $P_{111i4}NTf_2$ is presented in Figure S2 in the Supporting Information when a 10 mV potential was applied until a steady-state current was reached and EIS spectra of the same cell shortly before and after polarization are measured. The average value of the transference number was determined as 0.39 ± 0.01 (Table S1, Supporting Information).

Figure S3 in the Supporting Information shows the polarization and EIS data of a Na symmetrical cell containing 75 mol% $NaNTf_2$ in $P_{111i4}NTf_2$. The $T_{Na}^+$ value in this case was found to be 0.22 ± 0.01 (Table S2, Supporting Information). These are significant transference numbers for Na+, equivalent to those measured in liquid systems.[47,48] The effect of composition on $T_{Na}^+$ and the decrease for the higher $NaNTf_2$ concentration is not fully understood at this stage, although it indicates that the other ionic species become more dominant charge carriers in this hybrid system at high Na salt concentration.

#### *2.3.3. Galvanostatic Cycling of Na/OIPC/Na Symmetrical Cells*

The ability of the electrolyte to cycle Na metal with good efficiency and without breakdown is a key factor for the practical use of OIPCs in Na batteries. To explore the behavior across the composition range for the materials of interest here, we have


© 2016 WILEY-VCH Verlag GmbH & Co. KGaA, Weinheim

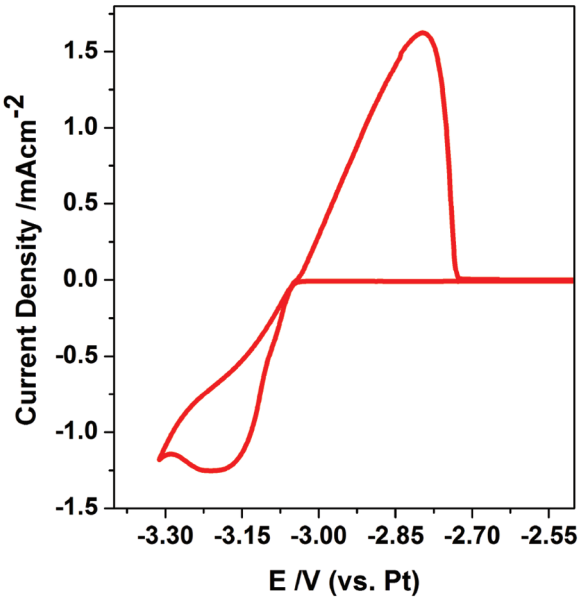


**Figure 3.** Cyclic voltammogram of 25 mol% of $NaNTf_2$ in pure $P_{111i4}NTf_2$ at 50 °C with a scan rate of 10 mV $s^{-1}$. Working electrode was Cu and reference/counter electrodes were both Pt.

chosen two concentrations of $NaNTf_2$ (25 and 75 mol%) which, although having similar conductivity, will present different ratios of liquid and solid phases. At any given temperature, the 25 mol% $NaNTf_2$ will have a larger fraction of liquid phase above the transition at 48 °C.

Sodium symmetrical cells, with 75 mol% $NaNTf_2$ in $P_{111i4}NTf_2$ were constructed and cycled at current density of 0.1 mA $cm^{-2}$ for 100 cycles at 50 °C with one hour for each step of charge and discharge (i.e., 0.1 mA h $cm^{-2}$ for each polarization step). The typical galvanostatic cycling results of these cells are presented in Figure S4 in the Supporting Information. For every cycle, the plating and stripping of Na metal led to a stable, low polarization plateau at 0.2 V. After approximately 15 min of current passing through the cell a rapid increase in potential up to the instrument limiting potential (±5 V for charge and discharge, respectively) occurred. Nevertheless, no breakdown or shorting was observed and the cell continued to operate well for all 100 cycles. This result represents the first time that an OIPC-based electrolyte has been demonstrated to perform in a Na device, and at such a high concentration of sodium salt, noting that the material is essentially in a solid state at this composition, although a small fraction of liquid (IL) phase will also be present within the solid structure (as indicated from the phase diagram Figure 1b). Given the solid-state nature of this electrolyte, the most likely reason for excessive polarization after around 15 min at 0.1 mA $cm^{-2}$ (corresponding to 90 mC of charge) is the depletion or saturation of Na ions in the electrolyte at the interface that prevents further electrochemical reactions proceeding.

Another experiment employing a cycling period of 10 min, at the same current density (0.1 mA $cm^{-2}$) and same temperature (50 °C) was also undertaken (Figure S5, Supporting Information). Under these conditions, the cell does not reach the potential limit and the polarization potential throughout the 10 min is constant at around 0.2 V. This also shows that the polarization potential for these symmetric cells remains quite stable and confirms excellent stability with this high $NaNTf_2$ concentration OIPC.

**Figure 4**a shows the voltage versus polarization capacity at 50 °C and 60 °C. A decrease in the polarization potential was observed with increasing the temperature, confirming that the cell performance is improved at 60 °C. Furthermore, this behavior indicates that the overall cell resistance at the 60 °C is lower than at 50 °C, as confirmed in the impedance plots in Figure S6 in the Supporting Information where a decrease in cell resistance was observed at the higher temperature. This suggests that a uniform solid electrolyte interphase (SEI) forms at the electrode surface that is stable and less resistive when the temperature is increased to 60 °C.

For comparison, a symmetric cell consisting of 25 mol% $NaNTf_2$ in $P_{111i4}NTf_2$ was assembled and cycled at 50 °C with at current density of 0.1 mA $cm^{-2}$ for 1 h each step of charge and discharge. In this case, the electrolyte will be mostly in the liquid phase as indicated by the phase diagram in Figure 1b. The results are shown in Figure S7 in the Supporting Information and Figure 4b indicate that, for this 25 mol% $NaNTf_2$ electrolyte, a low polarization potential (approximately 0.05 V) is achieved during the entire 45 h of cycling. According to the conductivity data in Figure 2, the $Na^+$ diffusivity is likely to be higher for 25 mol% compared with that for 75 mol% $NaNTf_2$ at the same temperature. The higher fraction of liquid phase leads to better conductivity, and possibly better interfacial contact, of the electrolyte which resulted in improved cell performance.

An improved cell performance was again observed upon increasing the temperature from 50 °C to 60 °C (Figure S8, Supporting Information). Figure 4b clearly shows the lower polarization potential of the cell at 60 °C compared to 50 °C for the 2nd, 5th, and 10th cycles suggesting an apparent lower interfacial resistance as confirmed by the impedance data for this cell (Figure S9, Supporting Information).

Preliminary full cell cycling using a $NaFePO_4$ cathode also shows the promise of these electrolytes in Na metal batteries as shown in Figure S10 in the Supporting Information. The initial cycling of the 25 mol% system delivers a capacity of 76 mA h $g^{-1}$ at C/10 rate with high efficiency. A similar value is obtained for very slow charge/discharge cycles in the case of the 75 mol% $NaNTf_2$. These numbers reflect less than full utilization of the active material (theoretical specific capacity 150 mA h $g^{-1}$) as the access of the electrolyte to the cathode particles has not been optimized in these solid-state materials. Significant improvements can no doubt be expected as the electrode/electrolyte combination is further developed and the electrode formulation is better matched to the unique solid-state electrolyte. It can be expected that formation cycles and thermal treatments may also be required to optimise the cathode utilization. Exploration of this and the effectiveness and efficiency of Na metal electrode cycling (as well as that of other Na insertion/alloying anodes) are clear topics for further research.

The more detailed morphology and structural characteristics of these mixed phase solid-state Na OIPC electrolytes is presented below. A discussion relating the temperature and composition-dependent morphology and electrochemical behavior will follow.


© 2016 WILEY-VCH Verlag GmbH & Co. KGaA, Weinheim

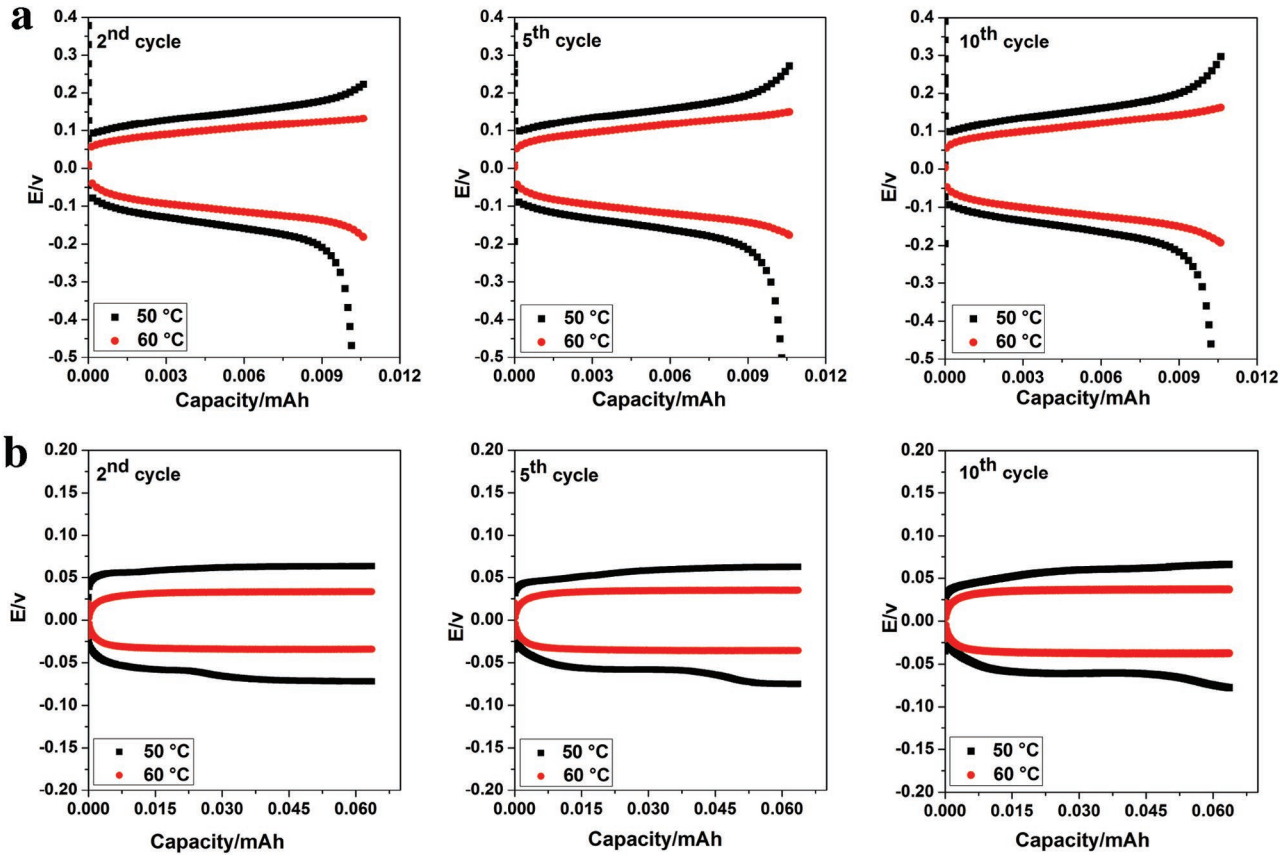


**Figure 4.** Charge/ discharge profiles for a) 75 mol%, b) 25 mol% $NaNTf_2$ in $P_{111i4}NTf_2$ cells, 2nd, 5th, and 10th cycles at two different temperatures (50 °C and 60 °C).

### 2.4. Morphology

In order to gain information about the topography and microstructure of the samples, scanning electron microscopy was performed on various composition of $(1-x)P_{111i4}NTf_2-(x)NaNTf_2$ at room temperature. The SEM image of pure OIPC (**Figure 5**a) distinctly shows the plastic properties of this material with slip planes observed as seen in previous OIPC examples.[24,41] At the eutectic composition (5%, Figure 5b) small particles (possibly $A_4B$, where A = OIPC and B = $NaNTf_2$) were dispersed within the matrix of mixtures. At 20% $NaNTf_2$, the morphology looks to be that of a plastic phase but we cannot say with certainty from this image whether it is a single phase morphology. We note that the phase diagram suggests that this composition is indeed a single phase and NMR experiments discussed later will confirm this. At 25% (Figure 5d), again two distinct phases can be seen. From Figure 5d–f, the number of small particles appears to be increasing from 25 to 50 mol% of $NaNTf_2$, which reflects the volume fraction of B phase increasing at concentrations beyond the 25 mol% composition. One can conceive that just above the peritectic temperature, the fine grains of the solid phase will be encompassed by a mobile amorphous or liquid component where ion conduction is likely to occur. However, we cannot completely rule out additional conductivity through the solid state at this stage.

### 2.5. Solid-State NMR Characterization

The phase behavior of the pure and sodium doped OIPC with various concentration of sodium salts were studied by solid-state NMR.

Multinuclear solid-state NMR is a powerful method to interrogate local structure within a material. Due to the fact that $^{19}F$ is only in the anion ($[NTf_2]^-$), $^{19}F$ MAS solid-state NMR is used to probe the anion structure and dynamics. $^{23}Na$ NMR is used to study the local environment and mobility of the $Na^+$ ions within the binary systems. For each of the sample compositions, the fluorine ($^{19}F$) spectra give different signals (**Figure 6**a) indicative of different anion environments in each sample. In the pure $P_{111i4}NTf_2$, only a single $^{19}F$ signal is observed suggesting one distinct anion environment. However, two different signals are observed in the pure $NaNTf_2$ spectrum even though it is a single phase, pure material. The same behaviors were reported previously for $[C_2mpyr][NTf_2]/NaNTf_2$ binary systems.[41] The two peaks in the $NaNTf_2$ spectrum are because different $CF_3$ environments exist in the $NaNTf_2$; this is related to the different conformations possible in the $NTf_2$ anion. Moreover, the broad peak in the $NaNTf_2$ spectrum indicates that ions are rigid and they maintain their different positions. On the other hand, in the pure OIPC the $CF_3$ groups rotate rapidly and occupy average positions on the NMR time scale, thus only a single resonance


© 2016 WILEY-VCH Verlag GmbH & Co. KGaA, Weinheim

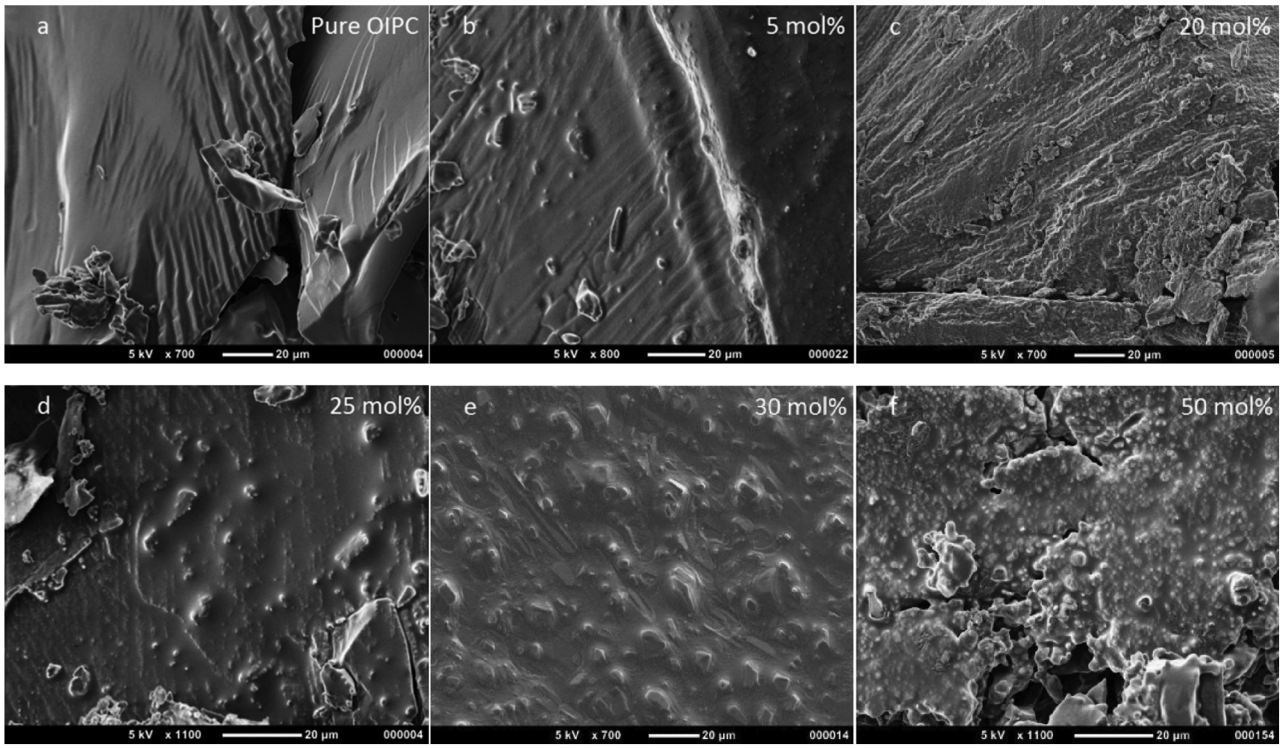


**Figure 5.** Binary system micrographs a) pure $P_{111i4}NTf_2$ OIPC, b) mixed with 5 mol%, c) 20 mol%, d) 25 mol%, e) 30 mol%, and f) 50 mol% $NaNTf_2$.

is observed. For the 5 mol% sample some small 'shoulders' are observed which become stronger at the 20% composition. Furthermore, a small signal at around –74 ppm begins to appear which is stronger in the 50 mol% sample. In the $^{23}Na$ spectra (Figure 6b), a quadrupolar line shape is observed in the pure $NaNTf_2$ spectrum. The neat $NaNTf_2$ shows signals that do not resemble those observed in the mixtures, especially the mixtures with the lower sodium content, indicating that the neat $NaNTf_2$ has a different structure or $Na^+$ environment. Given that the signals for the 50 mol% sample are similar to a combination of pure $NaNTf_2$ and the 20 mol% spectrum, two different phases exist in this composition, one of which should be the $NaNTf_2$ rich phase and the other is likely a new compound with $A_4B$ stoichiometry. Interestingly, the spectrum for 25 and 20 mol% are very similar, although the shoulder for the 25 mol% $NaNTf_2$ suggests the presence of some fraction of the

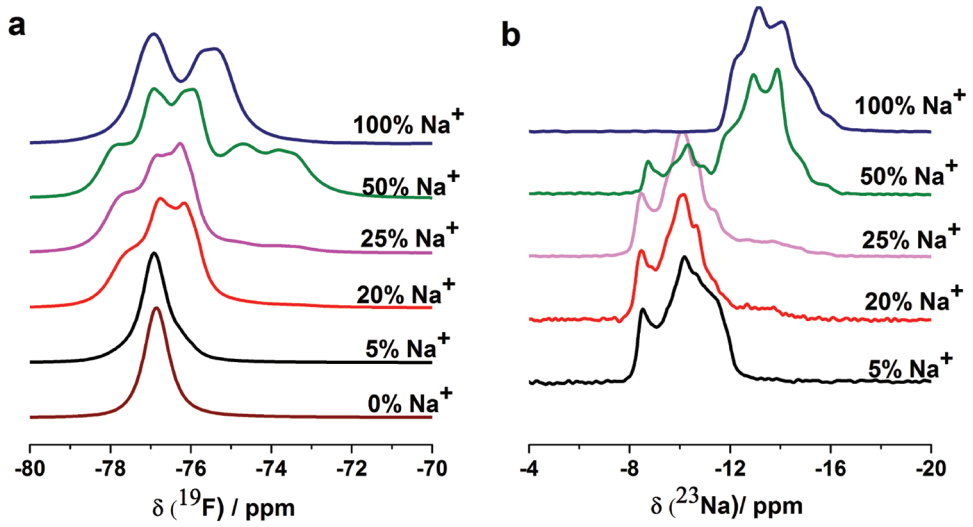


**Figure 6.** a,b) $^{19}F$ and $^{23}Na$ MAS solid-state NMR spectra for the binary mixtures from 0 to 100 mol% $Na^+$ content respectively.


© 2016 WILEY-VCH Verlag GmbH & Co. KGaA, Weinheim

$NaNTf_2$ rich phase. The spectrum for the 5 mol% sample also resembles the 20 mol% spectrum, with some small differences which are due to the presence of OIPC rich phase.

Further detailed investigations to understand the structure of the different phases using the combination of solid-state NMR and SXRD are on-going and will be published separately. The analysis presented thus far supports the phase diagram description above (Figure 1b) which indicates limited solubility at either end of the composition range and a stoichiometric compound at 4:1 OIPC: $NaNTf_2$ with a peritectic melt at 45 °C.

### 2.6. Correlation Between Electrolyte Morphology and Sodium Electrochemistry

**Figure 7** shows a schematic of the morphology expected in these electrolytes above the peritectic transition at 48 °C. The white, crystalline regions provide the solid-state properties of the material and the blue, intergranular regions contain mobile, Na rich ion liquid electrolyte leading to high ionic conductivity which supports the sodium electrochemistry and device cycling. This morphology will be dependent both on temperature and on composition. At higher temperatures, the volume of mobile interconnected domains will extend further into the white crystalline particles, which will essentially 'melt' or dissolve into the mobile phase. With higher $NaNTf_2$ concentration and at lower temperatures, the morphology above the peritectic will be closer to Figure 7 (left), whereas with increasing temperature and lower initial $NaNTf_2$ content, a larger fraction of the material will be a mobile liquid phase. This has significant implications for the electrolyte during cycling; with sodium plating from the electrode/electrolyte interface, the sodium content will be depleted whereas during discharging, the sodium content in the interfacial region will increase. Given the complex nature of the electrolyte phase behavior, we would expect this to change the morphology. Indeed, we have seen prior evidence in the case of OIPC electrolytes mixed with low concentration of lithium salt, that cycling of a lithium device leads to preconditioning and improvement of the metal/solid electrolyte interface.[7,30] What differentiates such solid electrolyte systems, particularly at these higher alkali metal salt concentrations, from a simple membrane impregnated with a sodium containing ionic liquid, is the availability of Na ions in the solid crystalline phase providing a reservoir of $Na^+$ which leads to a highly dynamic interface. There is great scope here to design the electrolyte morphology and composition to provide improved interfacial properties leading to better Na devices.

## 3. Conclusion

This work has demonstrated for the first time the cycling of a sodium electrochemical cell incorporating a plastic crystal electrolyte. The mixtures of the OIPC with high concentrations of alkali metal salts (up to 75 mol% $NaNTf_2$ in this case) result in high ionic conductivity, even in a predominantly solid phase, supporting stable electrochemical cycling of sodium. At 25 mol% $NaNTf_2$ (still significantly higher than typical electrolyte concentrations), we show for the first time, stable Na cycling in a phosphonium-based system, with high transference number for $Na^+$. Full Na/25 mol% $NaNTf_2$/$NaFePO_4$ cells were demonstrated at 50 °C with stable discharge capacities of ≈76 mA h $g^{-1}$. These observations clearly indicate the possibility of using such materials in sodium devices.

In addition to the electrochemical behavior, this work reports detailed thermal phase behavior and morphology across the entire composition range for $P_{111i4}NTf_2$ and $NaNTf_2$. As with the pyrrolidinium/sodium mixtures, the eutectic transition (at 63 °C) was not depressed as significantly upon addition of the sodium salt as for the equivalent lithium systems.[29] This allows for the preparation of ambient temperature solid-state electrolytes and hence construction of safe solid-state devices.

## 4. Experimental Section

*Sample Preparation:* *Tri*methylisobutylphosphonium bis(*tri*fluoromethylsulfonyl)amide ($P_{111i4}NTf_2$) was synthesized by Cytec Canada Inc. (CYTEC) with > 99.5% purity. It was dried under vacuum at

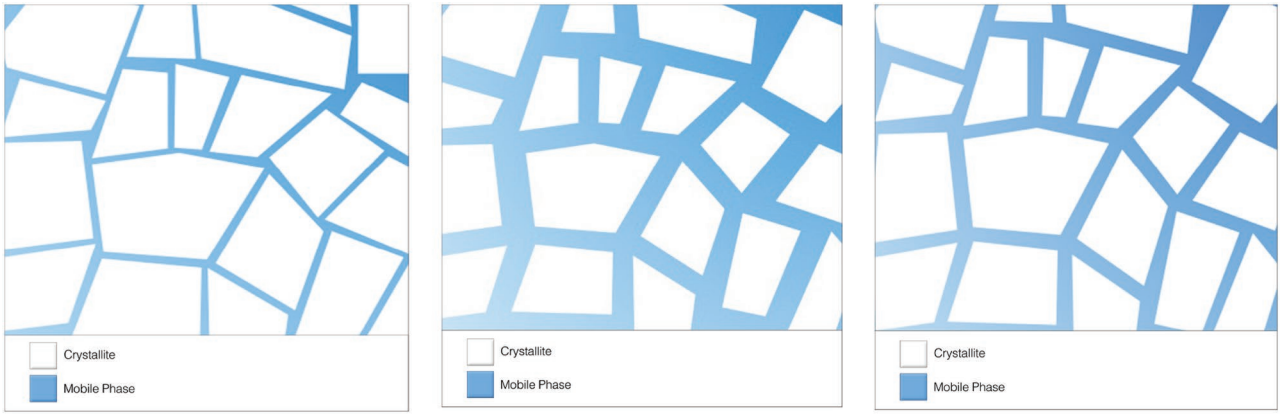


**Figure 7.** Schematic illustrating the mixed phase electrolytes with conductivity occurring predominantly along the mobile phase (shown in blue) between the crystalline regions (shown in white). The size of the crystalline regions and the width of the mobile domains will be dependent both on temperature and composition. The left schematic illustrates lower temperature and higher $Na^+$ concentration, whereas the rightmost schematic is the morphology expected at higher temperatures where more mobile phase is present.


© 2016 WILEY-VCH Verlag GmbH & Co. KGaA, Weinheim

80 °C for three days in the presence of Sodium hydride (NaH). Water content was checked by Karl Fischer to be less than 50 ppm. Sodium bis(*tri*fluoromethylsulfonyl)amide ($NaNTf_2$) (99.99%) was purchased from Solvionic company and used as received. Due to moisture sensitivity of both materials, they were held under an argon environment in a glove box. Different concentrations of $P_{111i4}NTf_2$/$NaNTf_2$ were prepared by adding the appropriate amount of salt into OIPC. Mixtures were stirred and heated to obtain a totally homogenous melt solution. Mixed samples were held in the vacuum oven for 5 h after obtaining the homogeneous solutions, then stored in hermetically sealed vials under an argon atmosphere inside the glove box. The chemical structure of $P_{111i4}NTf_2$ are presented in **Figure 8**.

*Differential Scanning Calorimetry (DSC)*: Thermal measurements were done by using a liquid $N_2$ cooled Mettler Toledo differential scanning calorimeter DSC822e and the data were analysed with STARe V6.10 software. The pans containing 3–5 mg of the samples were prepared inside the argon glove box and sealed to avoid air/moisture ingress into samples. Typically, the samples were cooled at 2 °C $min^{-1}$ from room temperature to –60 °C, heated to 70 °C for some compositions and up to 250 °C for other sample compositions. All samples were held at –60 °C for 10 min to equilibrate prior to heating. The heating traces are reported in this paper.

*Electrochemical Impedance Spectroscopy (EIS)*: Ionic conductivity of the samples was measured using electrochemical impedance spectroscopy with a Biologic MTZ –35 Analyser driven by MT-Lab software. Data were collected over a frequency range of 10 MHz to 1 Hz with a voltage amplitude of 0.1 V and over a temperature range of –20 °C to 70 °C at 10 °C intervals. A custom designed dip cell containing two platinum wires covered by glass was used to measure the ionic conductivity of samples. The cell constant was calibrated with a solution of 0.01 M KCl at 25 °C. The temperature was controlled using a Eurotherm 2204 temperature controller connected to the MTZ-35 and the sample temperature was measured by thermocouple in the blocking electrode. 20 min equilibration time was used to stabilise the temperature before each measurements. Decreasing the temperature below the room temperature was achieved by using liquid $N_2$ or dry ice pellets. All processes of cell preparation were conducted inside an argon-filled glove box.

*Cyclic Voltammetry (CV)*: Cyclic voltammetry was performed to investigate the redox behavior of sodium in 25 mol% $NaNTf_2$ doped $P_{111i4}NTf_2$. CV was carried out with a three-electrode system using a BioLogic SP–200 potentiostat. The whole processes, including preparation of the cell and electrochemical measurements, were performed in an argon-filled glove box. A 3 mm diameter Cu electrode was used as a working electrode and a platinum wire as counter and pseudo-reference electrodes. A scan rate of 10 mV $s^{-1}$ was applied. Before each experiment the surface of the working electrode was polished with 0.05 mm alumina powder on a polishing cloth and rinsed in distilled water and ethanol before drying in the oven at 70 °C for one hour. Both reference and counter electrodes were rinsed with distilled water and ethanol and subsequently dried in an oven at 70 °C for one hour before use.

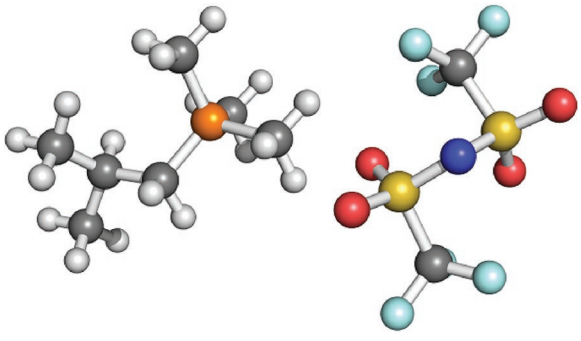

**Figure 8.** Chemical structure of $[P_{111i4}]^+$ (left-hand side) $[NTf_2]^-$ (right-hand side).

*Transference Number*: Na transference number was measured for 25 and 75 mol% NaFSI in $P_{111i4}NTf_2$ at 50 °C using a potentiostatic polarization method described by Evans et al.[45,46] 10 mV potential was applied to the cells and initial and steady-state currents were determined. The electrode resistance was measured by impedance just before and after polarization. All symmetric cell polarizations were carried out using a VMP3/Z Multi Potentiostat (Bio-Logic Science Instruments). EC-Lab software version 10.38 was used for fitting the EIS spectra.

*Symmetric Cell Cycling*: Na symmetric electrochemical coin cells were constructed using an electrolyte consisting of 75 and 25 mol% $NaNTf_2$ in $P_{111i4}NTf_2$ and cycled at 0.1 mA $cm^{-2}$ current density at 50 °C and 60 °C for 1 h for each polarization. A Biologic VMP3/Z potentiostat was used to cycle the cells galvanostatically and data were collected using EC-lab software. The charge and discharge cut-off voltage was ±5 V. Na symmetric cells were constructed to investigate the ability of the electrolyte to cycle Na metal with good efficiency.

Glass-fiber separators were dried under vacuum at 100 °C overnight and saturated by the melted electrolyte. After the separator was sufficiently wetted the temperature was decreased to 50 °C to solidify the electrolyte. This electrolyte was then sandwiched between two 9 mm diameter Na metal disks and assembled in a stainless steel cell case (Hohsen). Cell assembly was performed inside an argon-filled glove box. A spring and spacer was also used to provide uniform contact between electrodes and electrolyte inside the cell.

*Scanning Electron Microscopy (SEM)*: Scanning electron microscopy was used to gain information about the topography and microstructure of the OIPC. SEM was performed with JCM– 5000 Neoscope (Jeol Ltd.) desktop SEM. Powder samples were put on a carbon tape inside the glove box and transferred inside the canister. To reduce the exposure of samples to air, they were flushed with $N_2$ gas whilst putting them into the vacuum chamber. The images were acquired using an accelerating voltage of 5 keV.

*Solid-State Nuclear Magnetic Resonance (NMR) Spectroscopy*: Solid-state NMR spectroscopy was done on a Bruker AVANCE III 500WB spectrometer equipped with a 2.5 mm magic-angle-spinning (MAS) probe. Samples were packed into standard zirconia MAS rotors of 2.5 mm OD inside an argon glove box. $^{19}F$ and $^{23}Na$ spectra were acquired at 470.6 and 79.4 MHz, respectively, under MAS of 25 kHz using single pulse excitation and an equilibrated sample temperature of 283 K. $^{19}F$ and $^{23}Na$ shifts are given relative to $CFCl_3$ and 1 M NaCl, calibrated via a solid NaF external reference.

## Supporting Information

Supporting Information is available from the Wiley Online Library or from the author.

## Acknowledgements

The authors acknowledge the ARC (Australian Research Council) for its financial support through Australian Laureate Fellowship FL110100013 (M.F.) and Fl120100019 (D.R.M.) and also a Deakin University postgraduate research scholarship (F.M.). The authors are really grateful to Molly Patton for her artistic efforts. The authors also acknowledge the ARC for support through the DP130101652 and Cytec for the phosphonium material used here.

Received: June 14, 2016
Revised: August 8, 2016
Published online:

[1] D. R. MacFarlane, J. Huang, M. Forsyth, *Nature* **1999**, *402*, 792.
[2] Z-B. Zhou, H. Matsumoto, *Electrochem. Commun.* **2007**, *9*, 1017.


© 2016 WILEY-VCH Verlag GmbH & Co. KGaA, Weinheim

[3] J. M. Pringle, P. C. Howlett, D. R. MacFarlane, M. Forsyth, *J. Mater. Chem.* **2010**, *20*, 2056.
[4] J. Sunarso, Y. Shekibi, J. Efthimiadis, L. Jin, J. M. Pringle, A. F. Hollenkamp, D. R. Macfarlane, M. Forsyth, P. C. Howlett, *J. Solid State Electrochem.* **2012**, *16*, 1841.
[5] Y. Shekibi, T. Ruther, J. Huang, A. F. Hollenkamp, *Phys. Chem. Chem. Phys.* **2012**, *14*, 4597.
[6] J. M. Pringle, P. C. Howlette, D. R. MacFarlane, M. Forsyth, *Phys. Chem. Chem. Phys.* **2013**, *15*, 1339.
[7] P. C. Howlett, J. Sunarso, Y. Shekibi, E. Wasser, L. Jin, D. R. MacFarlane, M. Forsyth, *Solid State Ionics.* **2011**, *2*, 73.
[8] L. Jin, P. C. Howlette, J. Efthimiadis, M. Kar, D. R. Macfarlaneac, M. Forsyth, *J. Mater. Chem.* **2011**, *21*, 10171.
[9] L. Jin, P. C. Howlette, J. M. Pringle, J. Janikowski, M. Armand, D. R. Macfarlane, M. Forsyth, *Energy Environ. Sci.* **2014**, *7*, 3352.
[10] P. Wang, S. M. Zakeeruddin, P. Comte, I. Exnar, M. Gratzel, *J. Am. Chem. Soc.* **2003**, *125*, 1166.
[11] P. Wang, Q. Dai, S. M. Zakeeruddin, M. Forsyth, D. R. MacFarlane, M. Gratzel, *J. Am. Chem. Soc.* **2004**, *126*, 13590.
[12] Q. Li, X. Chen, J. Zhao, L. Qiu, Y. Zhang, B. Sun, F. Yan, *J. Mater. Chem.* **2012**, *22*, 6674.
[13] M. Yoshizawa-Fujita, K. Fujita, M. Forsyth, D. R. MacFarlane, *Electrochem. Commun.* **2007**, *9*, 1202.
[14] U. A. Rana, B. M. Bayley, R. Vijayaraghavan, P. C. Howlette, D. R. Macfarlane, M. Forsyth, *Phys. Chem. Chem. Phys.* **2010**, *12*, 11291.
[15] U. A. Rana, M. Forsyth, D. R. MacFarlane, J. M. Pringle, *Electrochim. Acta* **2012**, *84*, 213.
[16] P. J. Timmermans, *J. Phys. Chem. Solids* **1961**, *18*, 1.
[17] Y. Abu-Lebdeh, A. Abouimrane, P.-J. Alarco, M. Armand, *J. Power Sources.* **2006**, *154*, 255.
[18] Y. Abu-Lebdeh, P.-J. Alarco, A. Abouimrane, L. Ionescu-Vasii, A. Hammami, M. Armand, *J. New Mat. Electrochem. Syst.* **2005**, *8*, 197.
[19] S. J. Pas, J. Huang, M. Forsyth, D. R. MacFarlane, A. J. Hill, *J. Chem. Phys.* **2005**, *122*, 064704–1.
[20] a) Y. Abu-Lebdeh, P. J. Alarco, M. Armand, *Angew. Chem.* **2003**, *42*, 4736; b) Y. Abu-Lebdeh, P. J. Alarco, M. Armand, *Angew. Chem. Int. Ed.* **2003**, *42*, 4499.
[21] A. J. Seeber, M. Forsyth, C. M. Forsyth, S. A. Forsyth, G. Annat, D. R. MacFarlane, *Phys. Chem. Chem. Phys.* **2003**, *5*, 2692.
[22] S. J. Pas, J. M. Pringle, M. Forsyth, D. R. MacFarlane, *Phys. Chem. Chem. Phys.* **2004**, *6*, 3721.
[23] Y. Shekibi, A. Gray-Weale, D. R. MacFarlane, A. J. Hill, M. Forsyth, *J. Phys. Chem. C* **2007**, *111*, 11463.
[24] Y. Shekibi, S. J. Pas, N. M. Rocher, B. R. Clare, A. J. Hill, D. R. MacFarlane, M. Forsyth, *J. Mater. Chem.* **2009**, *19*, 1635.
[25] T. Chimdi, D. Gunzelmann, J. Vongsvivut, M. Forsyth, *Solid State Ionics.* **2015**, *272*, 74.
[26] J. Janikowski, C. Forsyth, D. R. MacFarlane, J. M. Pringle, *J. Mater. Chem.* **2011**, *21*, 19219.
[27] W. A. Henderson, V. G. Young, S. Passerini, P. C. Trulove, H. C. De Long, *Chem. Mater.* **2006**, *18*, 934.
[28] W. A. Henderson, M. Herstedt, V. G. Young, S. Passerini, H. C. De Long, P. C. Trulove, *Inorg. Chem* **2006**, *45*, 1412.
[29] D. R. MacFarlane, M. Forsyth, P. C. Howlett, M. Kar, S. Passerini, J. M. Pringle, H. Ohno, M. Watanabe, F. Yan, W. Zheng, S. Zhang, J. Zhang, *Nat. Rev. Mater.* **2016**, *1*, 15005.
[30] P. C. Howlett, Y. Shekibi, D. R. MacFarlane, M. Forsyth, *Adv. Energy. Mater.* **2009**, *11*, 1044.
[31] K. Romanenko, L. Jin, L. A. Madsen, J. M. Pringle, L. A. O'Dell, M. Forsyth, *J. Am. Chem. Soc.* **2014**, *136*, 15638.
[32] L. Jin, K. M. Nairn, C. M. Forsyth, A. J. Seeber, D. R. MacFarlane, P. C. Howlett, M. Forsyth, J. M. Pringle, *J. Am. Chem. Soc.* **2012**, *134*, 9688.
[33] K. Yoshii, K. Yamaji, T. Tsuda, K. Tsunashima, H. Yoshida, M. Ozaki, S. Kuwabata, *J. Phys. Chem. B* **2013**, *117*, 15051.
[34] K. Tsunashima, M. Sugiya, *Electrochem. Commun.* **2007**, *9*, 2353.
[35] K. J. Fraser, D. R. MacFarlane, *Aust. J.Chem.* **2009**, *62*, 309.
[36] V. Armel, D. Velayutham, J. Sun, P. C. Howlett, M. Forsyth, D. R. MacFarlanea, J. M. Pringle, *J. Mater. Chem.* **2011**, *21*, 7640.
[37] C. Pozo-Gonzalo, A. A. J. Torriero, M. Forsyth, D. R. MacFarlane, P. C. Howlett, *J. Phys. Chem. Lett.* **2013**, *4*, 1834.
[38] C. Pozo-Gonzalo, C. Virgilio, Y. Yan, P. C. Howlett, N. Byrne, D. R. MacFarlane, M. Forsyth, *Electrochem. Commun.* **2014**, *38*, 24.
[39] M. Kar, T. J. Simons, M. Forsyth, D. R. MacFarlane, *Phys. Chem. Chem. Phys.* **2014**, *16*, 18658.
[40] C. Pozo-Gonzalo, in *Electrochemistry in Ionic Liquids*, Vol. *2* (Ed: A. A. J. Torriero), Springer International, Switzerland **2015**, pp. 507–529.
[41] M. Forsyth, T. Chimdi, A. Seeber, D. Gunzelmann, P. C. Howlett, *J. Mater. Chem. A.* **2014**, *2*, 3993.
[42] W. D. Callister, *Materials Science and Engineering*, Wiley, New York **1940**, p. 312.
[43] W. A. Henderson, D. M. Seo, Q. Zhou, P. D. Boyle, J.-H. Shin, H. C. De Long, P. C. Trulove, S. Passerini, *Adv. Energy Mater.* **2012**, *2*, 1343.
[44] H. Yoon, H. Zhu, A. Hervault, M. Armand, M. Macfarlane, M. Forsyth, *Phys. Chem. Chem. Phys.* **2014**, *16*, 12350.
[45] P. G. Bruce, C. A. Vincent, *J. Electroanal. Chem.* **1987**, *225*, 1.
[46] J. Evans, C. A. Vincent, P. G. Bruce, *Polymer* **1987**, *28*, 2324.
[47] H. Yoon, H. Zhu, A. Hervault, M. Armand, D. R. MacFarlane, M. Forsyth, *Phys. Chem. Chem. Phys.* **2014**, *16*, 12350.
[48] C. Ding, T. Nohira, R. Hagiwara, K. Matsumoto, Y. Okamoto, A. Fukunaga, S. Sakai, K. Nitta, S. Inazawa, *J. Power Sources* **2014**, *269*, 124.


© 2016 WILEY-VCH Verlag GmbH & Co. KGaA, Weinheim